Eidgenössische Technische Hochschule Zürich
Swiss Federal Institute of Technology Zurich

Michel D. Heusser

# Identification of Acoustic Models for Active Noise Control of Motorcycle Helmets

**Semester Thesis**

Automatic Control Laboratory
Swiss Federal Institute of Technology (ETH) Zurich

**Supervision**

Prof. Dr. Roy S. Smith

March 2014

# Preface

I would like to thank Mr. Tony Wood, MSc. ETH Zurich, Ph.D. Student ETH Zurich, who was a very helpful advisor.

# Contents

# Abstract

System identification is the concept of developing mathematical models of dynamical systems from experimental data. In this project, we consider data from experimental measurements performed on a motorcycle helmet to derive acoustic models for active noise control. High noise levels in helmets are a major health concerns for occupational motorcyclists. Providing good noise attenuation would lower the risk of hearing loss.

Recent work on active noise control for motorcycle helmets suggests, that combining feedback and predictive feed-forward control techniques can lead to promising results. Such methods involve two acoustic models, which characterize the relationship of the sound at different points in the helmet. The quality of these models is crucial for the control performance. The data used in this report consists of microphone recordings from a series of experiments involving two different types acoustic excitations: white noise and swept sine signals. Two discrete system identification techniques were used to derive such models from given data. The first technique is non-parametric and calculates the discrete data of an empirical transfer function, which is then smoothed to reduce the effects of noise. The second one uses subspace identification techniques, specifically the N4SID algorithm, which derives a parametric state-space description of the models from the previously calculated smoothed empirical functions calculated before.

# 1. Introduction

## 1.1 Motivation

Due to a recent legislative regulation of noise in work environments, active noise cancellation in motorcycle helmets has gained increased attention in the last years. With the goal of preventing noise induced hearing loss (NIHL), a recent European court order has set the maximum noise level for a worker to tolerate during a regular working day to 87 dB. These regulations are very difficult to fulfill with existing technologies. Moreover, occupational motorcyclists of all kinds are specially at high risk of NIHL. This is why the search for possible technical innovations to enhance noise cancellation has become a pressing issue in the face of these recent developments (For more details on the topic please refer to [1] and [3]).

## 1.2 Objectives

The approach stated in [1] proposes the combination of a feed-forward controller with a feedback controller for satisfactory noise-canceling results, with the special consideration of the critical frequency band between 20 Hz and 1.5 kHz where the highest sound pressure levels are perceived[1]. This study has the objective of modeling the acoustic systems for both controllers, and subsequently performing system identification on them using externally gathered data.

## 1.3 Organization

In Chapter 2, I will describe the detailed acquisition and characteristics of the measured data obtained for this study. After having introduced the experimental parameters, I will show and explain the block diagrams (Section 2.3) describing the system models for the acoustic feed-forward and feedback setups. Chapter 3 will explain the details of the system identification techniques chosen for this study and their results using the external data. In the last part (Chapters 4 and 5) I will discuss the results and show my conclusions.

# 2. Data Acquisition

## 2.1 Experimental Setup

The data acquisition was done by Prof. Sánchez Peña ([1] and [3]), from the Instituto Tecnológico de Buenos Aires, who originally requested a system description of the acoustic setups. During the experiments, three different people and two different setups - one for the feedback controller and one for the feed-forward controller - were used. For the feed-forward setup, the first microphone was placed on the chin of the user and the second one in the ear canal, both inside the helmet (Figure 2.1). An external speaker, placed in front of the user, was then used to produce the sound-waves to be measured. Both signals of the microphones were saved in the channels of a stereo audio file without compression (44.1 kHz/16 bit).

For the feedback setup, only one microphone was placed in the ear canal (inside the helmet). The sound was then generated by a headphone outside the helmet at ear level (Figure 2.2). The

[1] The typical audible range of human hearing is 20 Hz to 20 kHz according to [1] and [2]

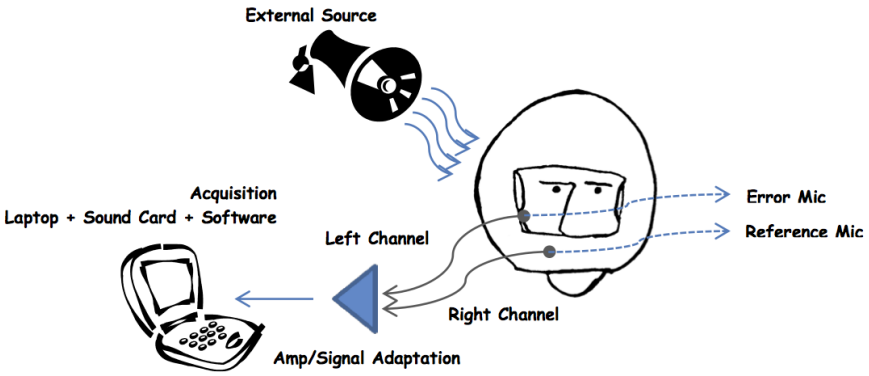


Figure 2.1: Acoustic Setup for the Feedforward Model

measured headphone voltage was the second recorded signal, which was also saved in a stereo audio file together with the ear microphone signal.

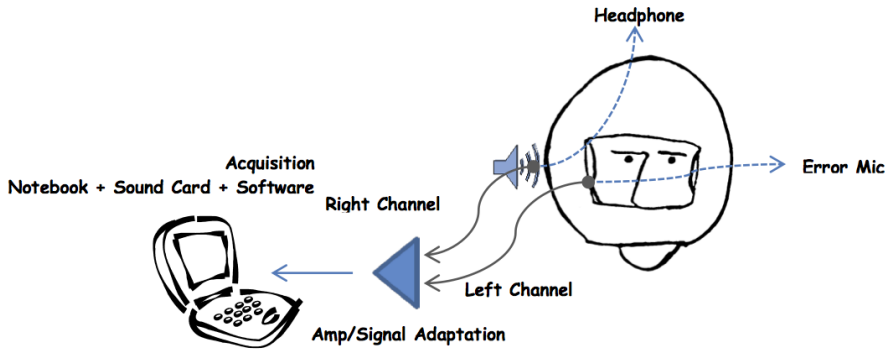


Figure 2.2: Acoustic Setup for the Feedforward Model

## 2.2 Input Signals

During the experiments, the speaker and headphone generated two types of signals for the measurements: A sinusoidal sweep, which gradually increases from 20 Hz to 4 kHz (Figure 2.4), and white noise run through a low pass filter with a cutoff frequency at 5 kHz (Figure 2.3). The sweep signal experiment was performed twice for each controller setup and the noise experiment only once. Everything was then repeated for the three different users. However, only one of the users delivered results of the desired quality. The two other users reported an uncomfortable fit, and the microphone's unintentional rubbing against the skin corrupted the signal. Therefore, I worked with only six pairs of measurements for the identification: Two sweep signals and one filtered noise signal, once for each controller setup.

## 2.3 System Modelling

In the feedback and feed-forward setups we are faced with an input-output behavior. We are interested in seeing how the sound pressure varies between the chin and the direct entry of the ear canal for the feed-forward setup, while the feeback setup examines the sound pressure behavior between the headphone and the ear canal. In the feed-forward setup, the sound wave at the chin would be the input signal, and the sound wave at the ear would be the output. In the case of the feedback setup, the sound wave created by the headphone would be the input and the sound wave at ear level the ouptut. The microphone measurements are corrupted by noise (which we assume

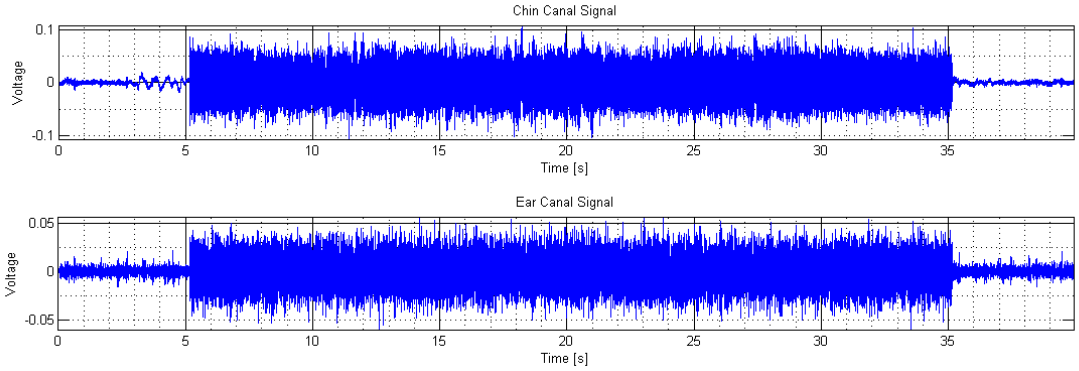


Figure 2.3: Filtered Noise Input Measurement with with the Feedforward Setup

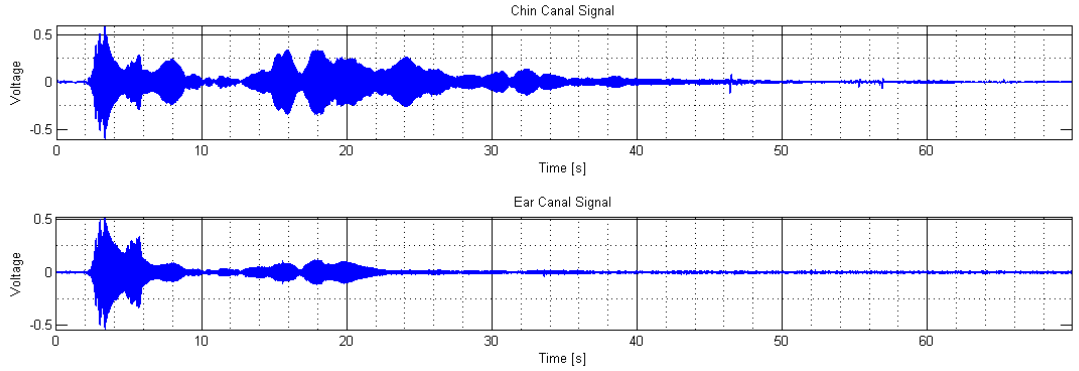


Figure 2.4: Sweep Sine Input Measurement with with the Feedforward Setup

to be white noise). Therefore, it is necessary to consider this assumption while choosing a suited model.

Figure 2.5 shows the block diagram for the feedback model. The signal chain starts with the analog voltage signal being fed to the headphone, which is corrupted by noise. The signal is then transferred into the computer as discrete data with an analog-to-digital converter (ADC). Inside the helmet, the sound wave is measured by a microphone, which adds noise, and then converted to discrete data with an ADC and a preamplifier.

Figure 2.6 illustrates the block diagram for the feed-forward model. The output data is the same as in the other model, but the input is different. The input of the signal chain is the analog sound wave coming from the speaker. The measured input data is given by the chin microphone - again with added noise - and is also converted to to a discrete signal by an ADC and a preamplifier.

The purpose of this analysis is to determine a model that describes the real acoustic system for control purposes, which in Figures 2.5 and 2.6 would be represented by the transfer function $G(s)$. Using a continuous model as the one mentioned above makes little sense in the context that a suited controller should be discrete, and thus would require a discrete system. The most logical approach is therefore the inclusion of the electronic setup in the system to be identified, since the use of a controller would anyways require a digital voltage signal as input-output data. The identification model that will be used in this study is therefore the one shown in Figure 2.7. Here, the transfer function will be discrete, as well as it's input and output, for both FF and FB cases.

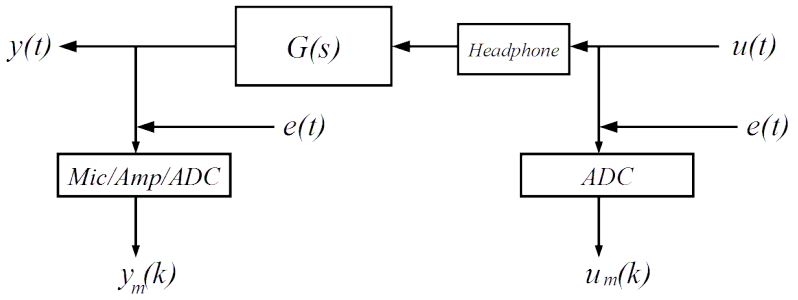


Figure 2.5: Block Diagram of the Acoustic Model for the Feedback Setup

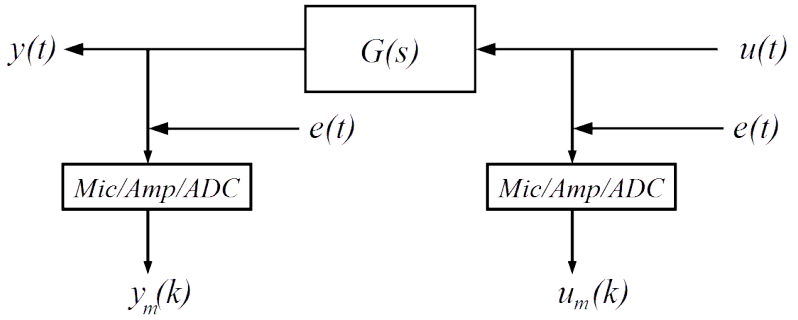


Figure 2.6: Block Diagram of the Acoustic Model for the Feed-forward Setup

These inputs and outputs are again corrupted by discrete white noise.

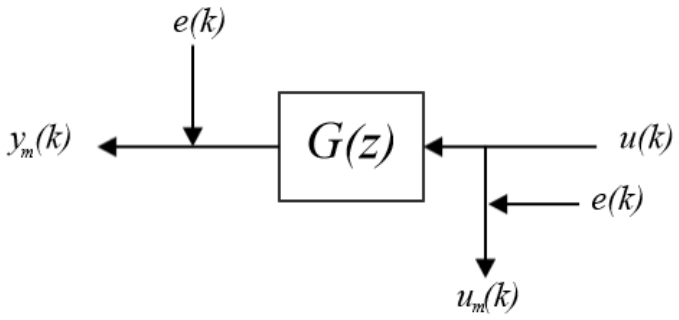


Figure 2.7: Discrete Model Used for the System Identification (FF and FB setups)

# 3. Analysis and Identification

In this chapter I will explain the mathematical methods used for the analysis of the data, with the purpose of finding the transfer functions that describe both systems. Basically, there are three main steps I took to find the transfer functions: Averaging, calculating a non-parametric transfer function, and subspace identification using the N4SID-Algorithm.

For the identification process mentioned above, I used the filtered white noise data, since we can average it and it contains information over a higher frequency range. To validate the identification, I used the sweep sign signals.

## 3.1 Averaging

Since white noise is an independent stochastic process (data points are uncorrelated), we can divide the whole measurement into independent data sequences. Averaging is an unbiased operation, helping to reduce the effect of noise. Therefore, we want to maximize the amount of times we subdivide the measurement. However, we don't want to lose resolution in the frequency steps, when doing a discrete Fourier transform.

The minimal frequency step we need equals the smallest relevant frequency, which is 20 Hz in our case. We then describe the frequencies in an N-point Fourier transform, using Herz (Hz) as a unit.

$$f_{\min} = \omega_k|_{k=1} \frac{f_S}{2\pi} = \left.\frac{2\pi k}{N}\right|_{k=1} \frac{f_S}{2\pi} = \frac{f_S}{N}$$

Now we can derive the needed amount of data points $N$ per subdivision to preserve the desired frequency resolution.

$$\Rightarrow N = \frac{f_S}{f_{\min}} = \frac{44100 \text{ Hz}}{20 \text{ Hz}} = 2205$$

Subsequently, we can divide the noise signals of both FF and FB setups into $N_s$ subdivisions of $N = 2205$ data points. A discrete Fourier transform will be used on every subdivision:

$$U_i(e^{j\frac{2\pi n}{N}}) = \frac{1}{N}\sum_{k=1}^{N} u_i(k)e^{-j\frac{2\pi n}{N}} \quad , \quad Y_i(e^{j\frac{2\pi n}{N}}) = \frac{1}{N}\sum_{k=1}^{N} y_i(k)e^{-j\frac{2\pi n}{N}}$$

for all $i = 1, ..., N_s$. Here is $u_i(k)$ the $i$th subdivision of the input signal, i.e. the chin signal in the FF model and headphone signal in the feedback model. Similarly $y_i(k)$ is the $i$th subdivision of the output signal, i.e. the ear signal for both models.[2]

Now, we can average each Fourier transformed signal:

$$U_{\text{av}}(e^{j\frac{2\pi n}{N}}) = \frac{1}{N_s}\sum_{k=1}^{N_s} U_i(k) \quad , \quad Y_{\text{av}}(e^{j\frac{2\pi n}{N}}) = \frac{1}{N_s}\sum_{k=1}^{N_s} Y_i(k)$$

Figure 3.1 shows the Fourier transform of the averaged and the non-averaged, complete, noise signal in the headphone channel and in the ear channel. We see a clear reduction of noise in the averaged one.

## 3.2 Empirical Transfer Function

After this, we can calculate the data points of the non-smoothed empirical transfer function $G_E(e^{j\frac{2\pi n}{N}})$ at the frequencies where the Fourier transformed signals are defined ([4]):

$$G_E(e^{j\frac{2\pi n}{N}}) = \frac{Y_{\text{av}}(e^{j\frac{2\pi n}{N}})}{U_{\text{av}}(e^{j\frac{2\pi n}{N}})}$$

[2] Although the calculation of the empirical transfer function was done following the steps in [4], I chosed another definition of the Fourier coefficients so that they are not scaled by any coefficient. Since we are ultimately calculating ratios between Fourier transformed values, this new definition gives the same results as in [4]

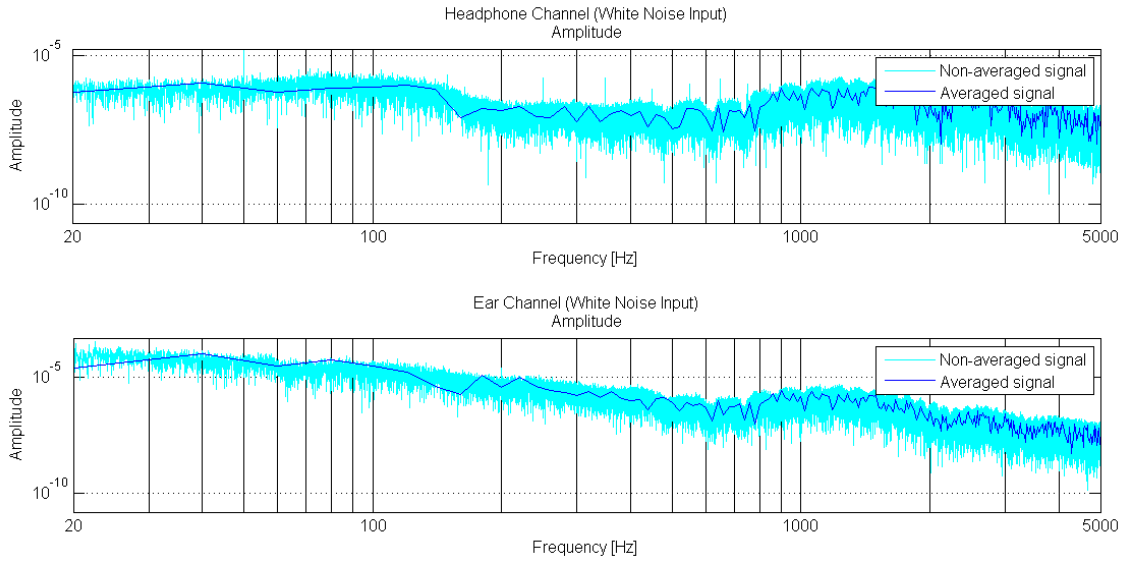


Figure 3.1: Fourier Transformed Filtered White Noise Measurements
(Averaged vs Non-averaged)

The empirical transfer function shows a noisy behavior, since our signals are corrupted with noise (it would otherwise show the actual data points of the transfer function). Since the algorithm we will use later to find the parametric description of the system (N4SID Algorithm) works best with data points of a smoothed estimate, we will smooth our empirical transfer function estimate.

First we must calculate the autocorrelation of $u(k)$ and cross-correlation of $u(k)$ and $y(k)$:

$$R_{yu}(k) = \frac{1}{N}\sum_{l=1}^{N} y(l)u(l-k) \quad , \quad R_u(k) = \frac{1}{N}\sum_{l=1}^{N} u(l)u(l-k)$$

It can be proved, that the empirical transfer satisfies the following relation:

$$G_E(e^{j\frac{2\pi n}{N}}) = \frac{\Phi_{yu}(e^{j\frac{2\pi n}{N}})}{\Phi_u(e^{j\frac{2\pi n}{N}})}$$

where $\Phi_{yu}(e^{j\frac{2\pi n}{N}})$ and $\Phi_u(e^{j\frac{2\pi n}{N}})$ are the Fourier transforms of the auto- and cross-correlations shown above. In order to smooth the transfer function we can introduce a window that reduces the correlation of each frequency data point only to the ones near it. This is consistent with the assumption that the transfer function is always locally smooth. It helps to reduce the chaotic jumping movement that noise causes.

I implemented the window $w_\gamma(k)$ in the time domain creating a smoothed discrete Fourier transform of the auto- and cross-correlation[3]:

$$\hat{\Phi}_{yu}(e^{j\frac{2\pi n}{N}}) = \frac{1}{N}\sum_{k=1}^{N} R_{yu}(k)w_\gamma(k)e^{-j\frac{2\pi n}{N}} \quad , \quad \hat{\Phi}_u(e^{j\frac{2\pi n}{N}}) = \frac{1}{N}\sum_{k=1}^{N} R_u(k)w_\gamma(k)e^{-j\frac{2\pi n}{N}}$$

The smooth transfer function $G_{\text{smooth}}(e^{j\frac{2\pi n}{N}})$ is[4].

[3] idem.

[4] It might seem, that the smoothing process doesn't need the initial empirical function as an input. However,

$$G_{\text{smooth}}(e^{j\frac{2\pi n}{N}}) = \frac{\hat{\Phi}_{yu}(e^{j\frac{2\pi n}{N}})}{\hat{\Phi}_{u}(e^{j\frac{2\pi n}{N}})}$$

### 3.2.1 Frequency Window

The window $w_\gamma(k)$, which was used above, is the inverse Fourier transform of the frequency weighted window $W_\gamma(\omega)$ (also called Parzen window), which has the following structure:

$$W_\gamma(\omega) = \frac{4 + 2\cos(\omega)}{\pi\gamma^3}\left(\frac{\sin(\frac{\omega}{4})}{\sin(\gamma\frac{\omega}{2})}\right)^4$$

and the following holds:

$$w_\gamma(k) = \int_{\pi}^{\pi} W_\gamma(\xi) e^{j\xi\frac{2\pi k}{N}} \mathrm{d}\xi$$

Figure 3.2 shows the shape of the frequency window for $\gamma = 5$.

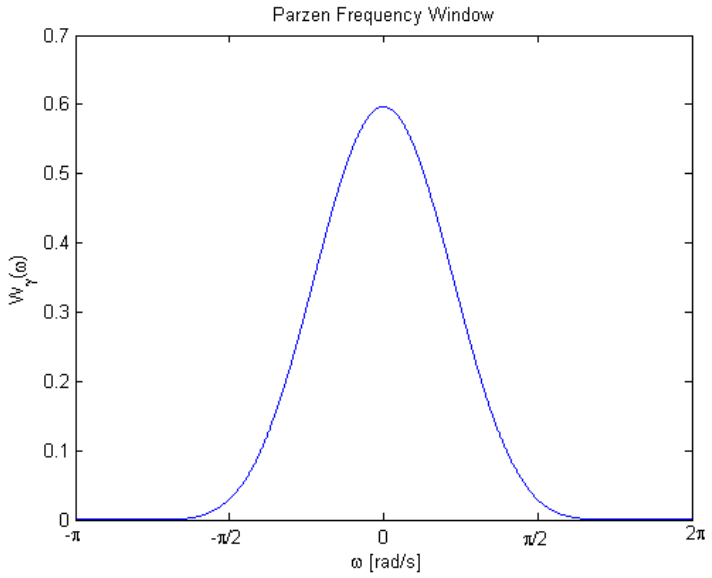


Figure 3.2: Parzen Window in the Frequency Domain for $\gamma = 5$

Here $\gamma$ is the parameter of smoothness ([4]). For $\gamma \to \infty$ the window $W_\gamma(\omega)$ has no effect. For $\gamma \to 0^+$ the smoothing becomes more prominent. The smoothing of the transfer function is generally a biased method, which tries to minimize its variance. Depending on the smoothing parameter $\gamma$, one could obtain a function with a high bias, but low variance (high smoothing), or low bias with a higher variance (low smoothing).

Figure 3.3 displays the Bode plot of the non-smoothed feed-forward transfer function estimate compared with smoothed estimates using different values of $\gamma$.

it can be proven that the method applied here, using the cross-correlation and autocorrelation of the data, is mathematically equivalent to convoluting the empirical non-smoothed transfer function with the frequency window $W_\gamma(\omega)$. Numerically, I found it easier to perform calculations with the method shown above. For further details please refer to [4]

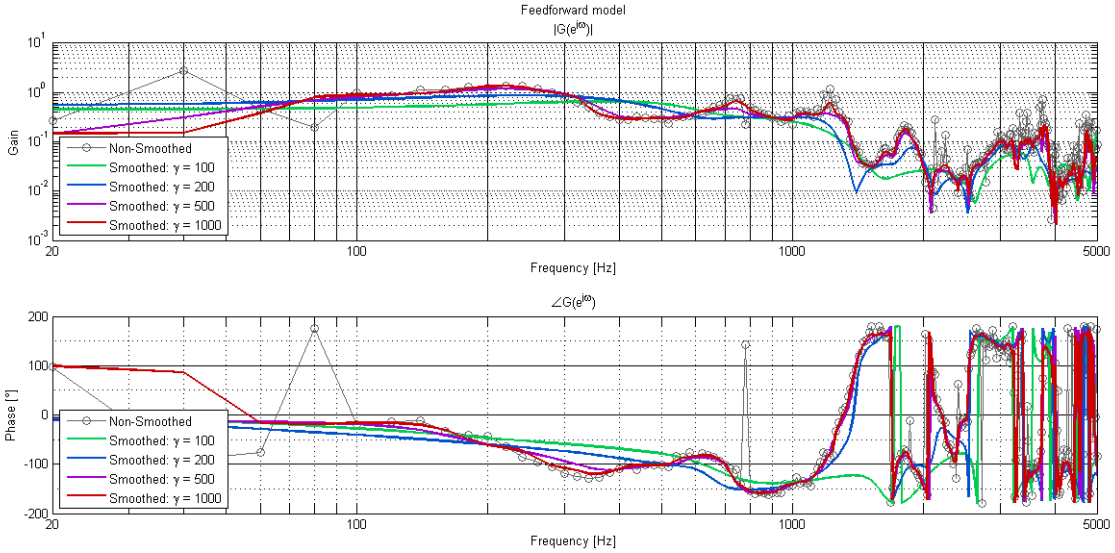


Figure 3.3: Comparison of Bode Plots Between Various Smoothed Estimates (FF Model)

## 3.3 Subspace Identification

Although linear systems are usually described in the frequency domain, state-space models can be used as a natural way of representing multi-variable parametric systems. Therefore, most implementations of control theory tools use state-space representations. There are a great number of algorithms that can be applied when time-domain measurements are available. Among the non-iterative algorithms we find the N4SID algorithm, an unbiased subspace identification algorithm that generates discrete state-space models without having to perform an explicit parameterization of the model set. The algorithm estimates subspace-based models, where the transfer function is rather insensitive to small changes in the matrix elements. This presents us with the possibility of identifying high order systems.

The method I used for the next part of the analysis uses the frequency domain identification algorithm proposed in [5] and [6], which uses samples of the transfer function and delivers a minimal state-space model. Singular value decomposition (SVD) of a noisy data matrix has to be performed a priori in order to optimize the system order. Only then can the algorithm be performed. The main advantages are the possibility of using a non-uniform frequency grid for the input frequency-domain data and its consistency (unbiased) over noise, as well as mathematical accuracy.

### 3.3.1 Order analysis and N4SID Algorithm

As mentioned above, the order of the system has to be known a priori in order to use the N4SID algorithm. The following calculations are performed. The noisy data matrix $\mathbf{G}$, as well as the complex matrix $\mathbf{W}_{\mathrm{m}}$ are defined:

$$\mathbf{G} = \frac{1}{\sqrt{M}} \begin{bmatrix} G_1 & G_2 & \dots & G_M \\ e^{j\omega_1} G_1 & e^{j\omega_2} G_2 & \dots & e^{j\omega_M} G_M \\ e^{j2\omega_1} G_1 & e^{j2\omega_2} G_2 & \dots & e^{j2\omega_M} G_M \\ \vdots & \vdots & \ddots & \vdots \\ e^{j(q-1)\omega_1} G_1 & e^{j(q-1)\omega_2} G_2 & \dots & e^{j(q-1)\omega_M} G_M \end{bmatrix}$$

and

$$\mathbf{W}_m = \frac{1}{\sqrt{M}} \begin{bmatrix} 1 & 1 & \dots & 1 \\ e^{j\omega_1} & e^{j\omega_2} & \dots & e^{j\omega_M} \\ e^{j2\omega_1} & e^{j2\omega_2} & \dots & e^{j2\omega_M} \\ \vdots & \vdots & \ddots & \vdots \\ e^{j(q-1)\omega_1} & e^{j(q-1)\omega_2} & \dots & e^{j(q-1)\omega_M} \end{bmatrix}$$

After this, a QR decomposition can be done in the following way:

$$\begin{bmatrix} \Re(\mathbf{W}_m) & \Im(\mathbf{W}_m) \\ \Re(\mathbf{G}) & \Im(\mathbf{G}) \end{bmatrix} = \begin{bmatrix} \mathbf{R}_{11} & 0 \\ \mathbf{R}_{21} & \mathbf{R}_{22} \end{bmatrix} \cdot \begin{bmatrix} \mathbf{Q}_1^T \\ \mathbf{Q}_2^T \end{bmatrix}$$

And a Cholesky decomposition in the following way:

$$\mathbf{K}\mathbf{K}^T = \alpha\, \Re(\mathbf{W}_p \,\mathrm{diag}(R_1, R_2, \dots, R_M)\mathbf{W}_p^*)$$

where $()^*$ represents the conjugate transpose operator. Finally we calculate the SVD in the following way:

$$\mathbf{K}^{-1}\mathbf{R}_{22} = U\Sigma V^T$$

Since we are only interested in seeing the relations between the singular values, the $\alpha$ parameter in the Cholesky decomposition is irrelevant. The values of $R_1, R_2, \dots$ correspond to the previously known co-variances of the noise. Since it was assumed that we are dealing with white noise, the covariance matrix must be some multiple of the identity matrix. In this context $\omega_1, \omega_2, \dots, \omega_M$ are the sampled frequencies of our transfer function. It is not a uniform grid, because we only have information up to 5 kHz, which lies below the nyquist frequency (22.05 kHz). The parameters $q$ and $p$ have to be chosen a priori and only have have to be larger than the order of the real system (without noise).

What we expect to see, is a discrepancy between singular values. This way, it should be easy to see how many belong to real states (order of the system) and which ones are "noise-states". As mentioned above, the N4SID Algorithm uses the order of the system, calculated with the SVD analysis, and the noisy transfer function samples calculated above.

### 3.3.2 Optimal Parameters

Unfortunately, the order analysis did not deliver any satisfactory results, since there is no clear discrepancy between singular values. The real order of the system therefore remains unclear. In the Appendix B one can see the singular value analysis for little, medium-level and a lot of smoothing for both setups. Since an order analysis was not possible to do, I took the approach of optimizing the parameters $\gamma$ and $n$ so that the rooth-mean-square error (RMS) in the relevant frequency band (20 Hz to 5 kHz) is minimized when validating with the sweep signal responses. In other words, I generated an estimated output signal while running the measured sweep sine input signal (in the headphone and chin microphone, for the FB and FF respectively) through the identified model. The root-mean-square error of the difference between the estimated and real output is calculated for each pair of $\gamma$ and $n$ in the following way:

$$(\hat{\gamma}, \hat{n}) \quad \text{s.t.} \quad RMS(\hat{\gamma}, \hat{n}) = \min_{(\gamma, n)} RMS(\gamma, n)$$

where:

$$RMS(\gamma, n) = \sqrt{\frac{1}{N_1 + N_2}\left(\sum_{i=1}^{N_1}(Y_1(e^{j\omega_i}) - Y_{\text{est},1}(e^{j\omega_i})) + \sum_{i=1}^{N_2}(Y_2(e^{j\omega_i}) - Y_{\text{est},2}(e^{j\omega_i}))\right)}$$

Here are $Y_1(e^{j\omega_n})$ and $Y_2(e^{j\omega_n})$ the real Fourier-transformed outputs (ear channel in each, the FB and the FF setup) for both sweep sign responses that were acquired for each setup. On the other hand, $Y_{\text{est},1}(e^{j\omega_n})$ and $Y_{\text{est},2}(e^{j\omega_n})$ are the estimated outputs with:

$$Y_{\text{est},1}(e^{j\omega_i}) = G_{est}(e^{j\omega_i})U_1(e^{j\omega_i}), \qquad Y_{\text{est},2}(e^{j\omega_i}) = G_{est}(e^{j\omega_i})U_2(e^{j\omega_i})$$

where $U_1(e^{j\omega_i})$ and $U_2(e^{j\omega_i})$ are the real measurements of the data inputs, Fourier-transformed and at the relevant frequencies, and $G_{est}(e^{j\omega_i})$ is the transfer function, evaluated at the relevant frequencies calculated from the state-space description delivered by the N4SID-algorithm.

A very important feature we want to have in the estimated model is stability. We want a model that is stable, and thus we have to search for the optimal parameters that also fulfill this prerequisite.

To analyze the RMS, I performed a search over all models of order $n = 1$ to $n = 20$, derived from a smoothed estimate of $\gamma = 10$ until $\gamma = 1000$, in incremental steps of 10. Since those models are going to be used for control purposes, we want to keep the order as low as possible, therefore it is unnecessary to search for orders higher than 20. For the smoothing parameter, I set the search limit to $\gamma = 1000$. As we see in Figures 3.3 and 3.4, smoothing parameters higher than 1000 over-fit the noisy response, which adds unnecessary information.

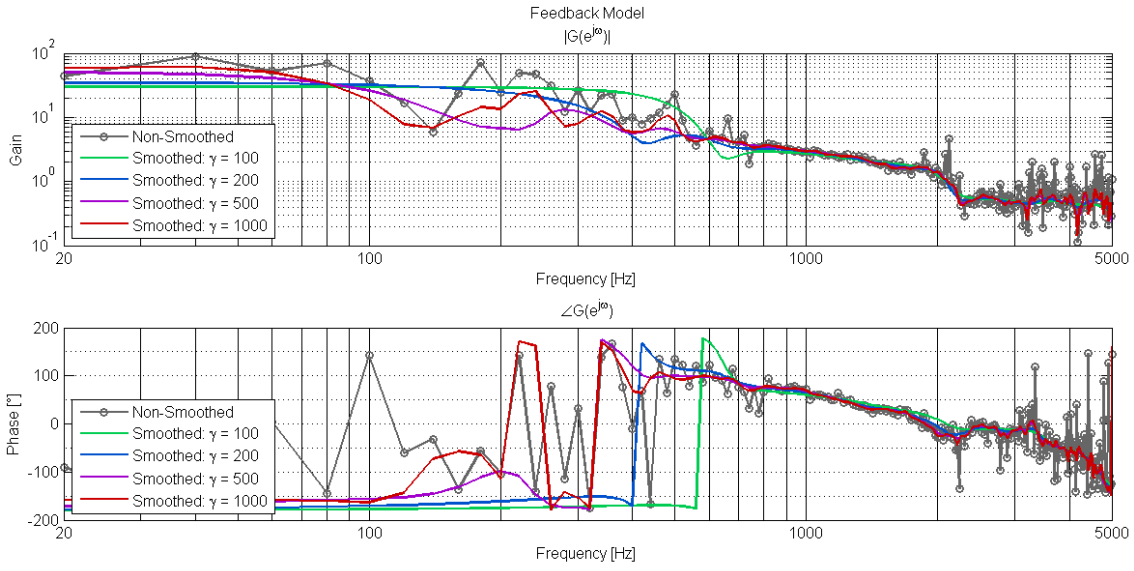


Figure 3.4: Comparison of Bode Plots Between Various Smoothed Estimates (FB Model)

# 4. Results and Discussion

## 4.1 Feedback Model

The optimization problem delivered the following result for the FB model:

| $\gamma$ | $n_{\text{order}}$ | RMS |
|---|---|---|
| 500 | 7 | 4.9381E-6 |

In Figure 4.1 we see the bode plot of the FB estimated system compared to the smoothed and noisy estimates. We see that until 3000 Hz, the final estimation follows the trend of the noisy response in amplitude and phase rather accurately. After that, the trend is followed with less accuracy by the estimated model. Towards 5 kHz, there is a roll-off in the estimation that is not observed in the trend of the noisy estimate. It is rather difficult to interpret the physical significance of the signal that this transfer function represents, since the input is the measured voltage applied to a headphone (not the actual measurement of the sound it produces) and the output is the sound inside the helmet. The fact that most of the transfer function has a higher gain than 1, doesn't mean, therefore, that the sound gets amplified. In fact, we would expect quite the contrary.

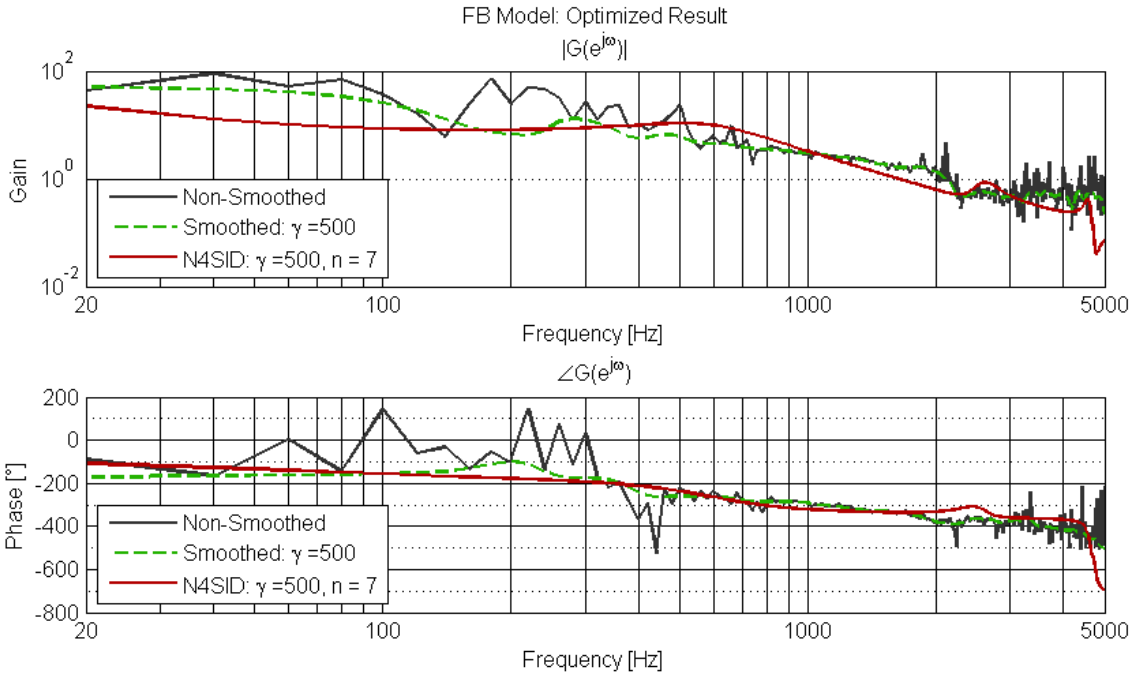


Figure 4.1: Resulting Estimates of the Parameter Optimization (Feedback Model) $\gamma = 500$ and $n = 7$

In the following plot (Figure 4.2) we see that the system is stable, since all of its poles are inside the unit circle of the Gauss-plane. As mentioned before, it is plausible to have assumed this a priori, since every frequency would eventually get damped to death inside of the helmet, even if there might be complex sound effects such as resonances or echoes. One of the poles is, however, much nearer to the unit circle axis. This leads to a slower roll-off of the impulse response, compared to the FF model, which will be described below. We also observe non-minimal phase zeros, which force the system to "lie" by letting it start in the opposite direction of the actual final behavior

observed in the impulse response (Figure 4.3a).

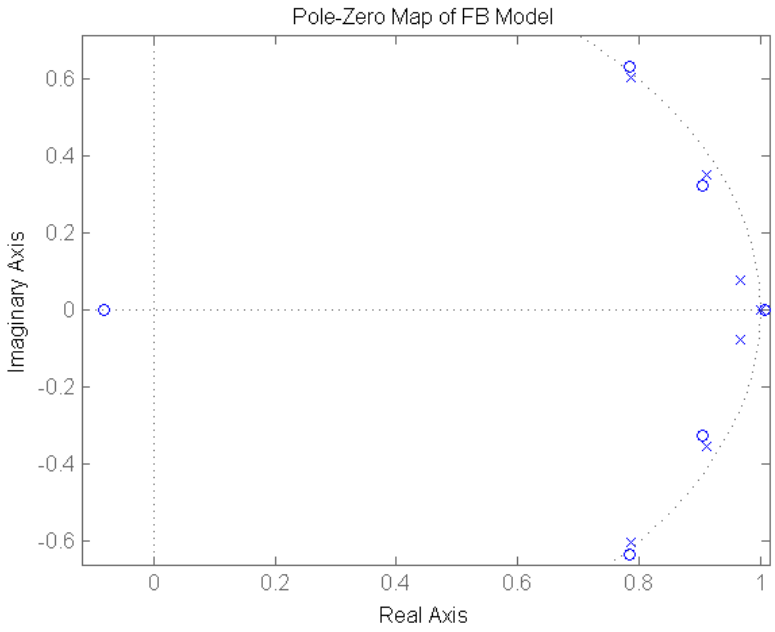


Figure 4.2: Poles (Cross) and Zeros (Circles) of the Identified Feedback Model

Initially, I didn't take in account the first 3 seconds of the filtered noise response into account to avoid including the transient part in the system identification process. Figure 4.3b shows, that the impulse response of the estimated model indeed decreases fast enough within the first 3 seconds to be able to assume, that the transient of the noise response is not present in the data that was taken for the identification.

## 4.2 Feedforward Model

For the feed-forward model identification we received the following result from our optimization problem:

| $\gamma$ | $n_{\text{order}}$ | RMS |
|---|---|---|
| 90 | 5 | 3.6571E-05 |

Figure 4.4 shows the bode plot of the estimated model compared to the smoothed and noisy models. The estimation here shows a better fit regarding the amplitude, but a more chaotic behavior in the phase plot. Due to the highly noisy behavior observed in the phase plot of the non-smoothed empirical function, the general trend of the curve is not clear and an unwrapping of the phase was not possible like it was done for the feedback model plot. The RMS in this case is almost one order greater than in the feedback model, which is clearly demonstrated by the phase plot. Fortunately, the estimated model follows the trend of the noisy and smoothed models much better in the amplitude plot than in the case of the feedback model. The result is therefore more satisfactory at lower and higher frequencies.

The bode plot always shows an amplitude lower than 1. This is what one would expect initially from the experiment, since the input signal comes from a source that closer to the sound source (chin channel) than the output (ear channel). Contrary to the feedback case, here are both input

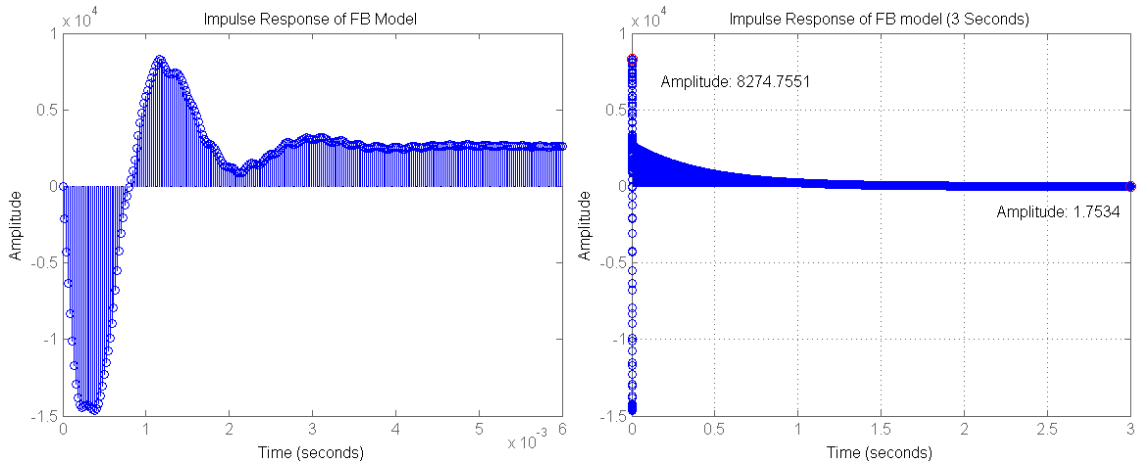


(a) (b)

Figure 4.3: Impulse Responses (Short-Term and Long-Term) for the Identified Feedback System

and output signals are voltage measurements of sound pressure.

Like in the FB case, we see in Figure 4.5 that the FF system's poles all lie within the unit circle. This time there are only minimal-phase zeros. We observe the stability provided by the poles, as well as no apparent systemic "lying" behavior in the impulse response, as shown by Figure 4.6a.

Figure 4.6b furthermore shows, that the assumption that the transient effect wears off within 3 seconds is plausible, since the amplitude decay decreases drastically within that time.

For detailed numerical information about the identified systems, i.e. transfer functions and system matrices, please refer to Appendix A.

Furthermore, a graphical demonstration of the optimization problem is presented in Appendix C. There, the RMS for every stable combination of the smoothing parameter $\gamma$ and order of the system $n$ is plotted.

# 5. Conclusion

As mentioned before, the results for both cases were very satisfactory in terms of following the trend of the noisy estimate in the critical noise frequency range from 20 Hz to 1.5 kHz (according to [1]), while preserving stability properties and low order. Since no further specifications were given that could give a better control performance, I find the optimization approach that minimizes the RMS satisfactory.

The models lack of accuracy in the higher frequency ranges used for identification. If one was to replicate our methods, i.e. smoothing and N4SID subspace identification, and aimed to achieve a higher accuracy, stability wouldn't be able to be preserved (better unstable fits were actually found). A possibility would be to perform more noise measurements and to only use averaging to smooth the function (if a higher range is desired, one would have to increase the cut-off frequency of

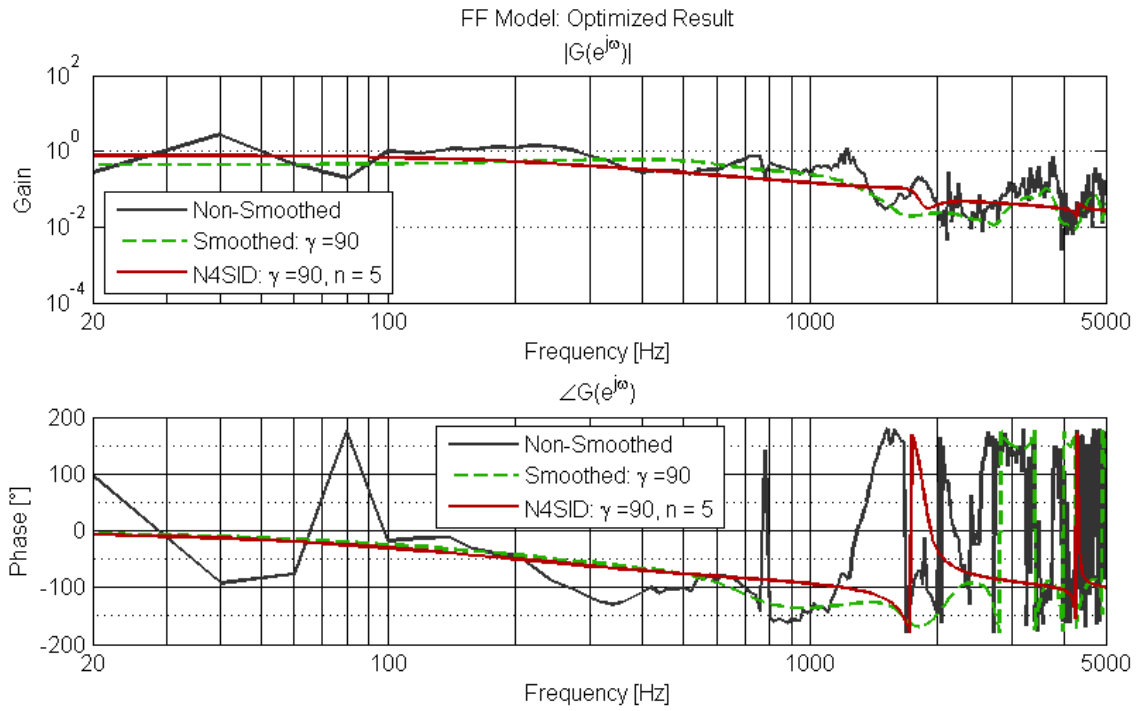


Figure 4.4: Resulting Estimates of the Parameter Optimization (Feed-forward Model) $\gamma = 90$ and $n = 5$

the filter on the white noise). This would be advantageous, since averaging is an unbiased method and smoothing is not. (I assumed tough, that the smoothed estimates have a low bias, in order to use the N4SID algorithm, which requires unbiased input responses in order to deliver an unbiased model).

Here, we dealt with a model that works with discrete inputs and outputs. If one was actually interested in the actual acoustic model that modifies the sound waves, one could use a bilinear transformation to create a continuous model. The relations between sound pressure levels at the microphone location and the amplitude of the signal it produces must be known to be able to derive this.

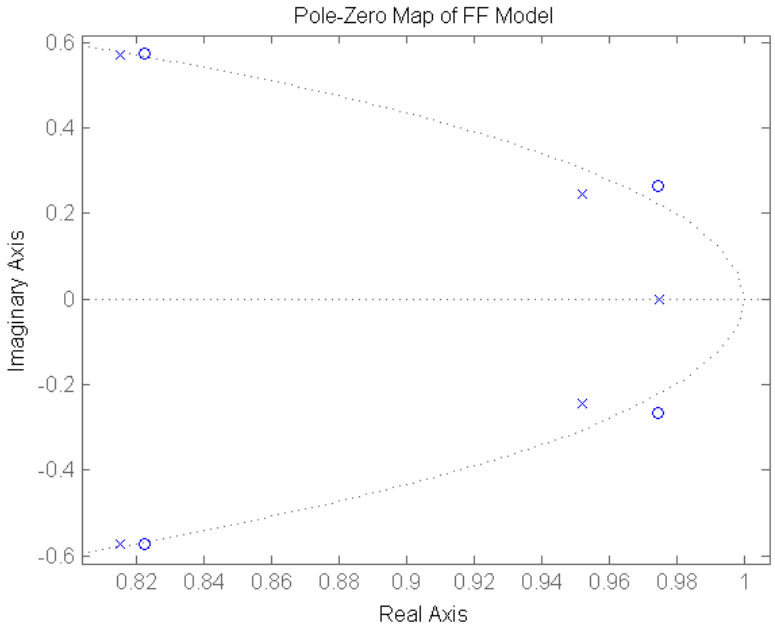


Figure 4.5: Poles (Cross) and Zeros (Circles) of the Identified Feed-forward Model

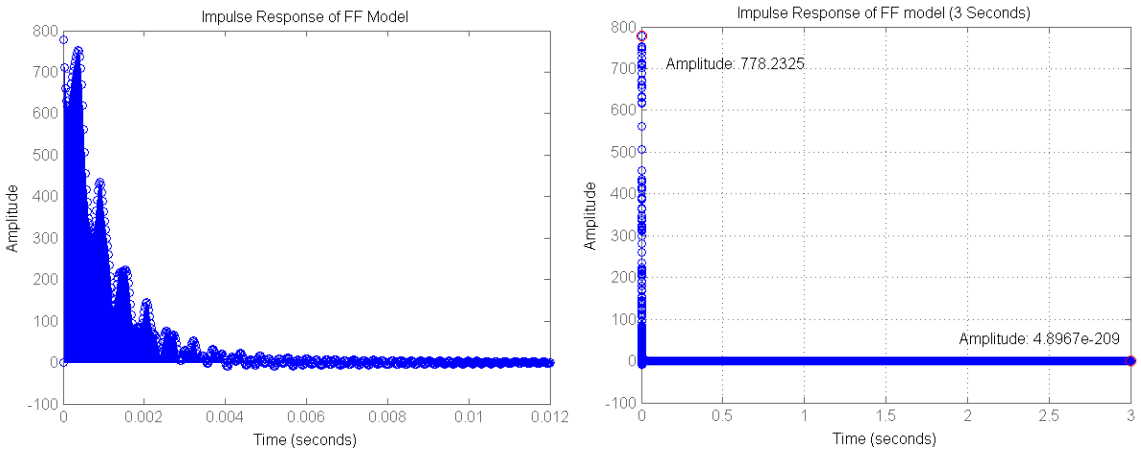


(a) (b)

Figure 4.6: Impulse Responses (Short-Term and Long-Term) for the Identified Feed-forward System

# A. Estimated Models

The models are described with the system matrices satisfying the following equation:

$$x(k+1) = Ax(k) + Bu(k)$$

$$y(k) = Cx(k) + Du(k)$$

where $x(k) \in \mathbb{R}^{7\times1}$, $u(k) \in \mathbb{R}$ and $y(k) \in \mathbb{R}$ for the FB case and $x(k) \in \mathbb{R}^{5\times1}$, $u(k) \in \mathbb{R}$ and $y(k) \in \mathbb{R}$ for the FF case.
The corresponding transfer functions $G(z)$ of both models are given as complex functions in the frequency domain (z-Transform).

## A.1 Feedback

System Matrices:

$$A = \begin{bmatrix} 0.9916 & -0.3021 & -0.01446 & -0.3975 & 0.3342 & 0.8979 & -1.751 \\ 1.014\cdot10^{-5} & 0.9818 & 0.5898 & 0.189 & -0.9155 & -1.135 & 2.958 \\ -0.0006971 & -0.02378 & 0.868 & 0.8622 & -0.4149 & -1.494 & 2.669 \\ 0.0001233 & 0.002188 & -0.1101 & 0.8439 & -1.218 & -0.9761 & 2.992 \\ 0.0001113 & 0.001061 & 0.007756 & 0.1362 & 0.8197 & 1.692 & -2.22 \\ 9.92410^{-6} & 0.0001823 & 0.004315 & -0.009561 & -0.08712 & 0.8108 & -2.475 \\ 4.18110^{-7} & -1.14310^{-5} & -2.11210^{-5} & 0.0001056 & 0.0008508 & 0.02776 & 1.011 \end{bmatrix} \quad B = \begin{bmatrix} -0.7629 \\ 0.3258 \\ -0.08028 \\ -0.01179 \\ 0.004377 \\ -0.00065 \\ -0.0001813 \end{bmatrix}$$

$$C = \begin{bmatrix} 0.3142 & 0.472 & -0.509 & 0.4186 & 0.3623 & -0.2782 & -0.1635 \end{bmatrix} \quad D = 0$$

Transfer Function:

$$G(z) = \frac{-0.0482z^{-1} + 0.2075z^{-2} - 0.3771z^{-3} + 0.3582z^{-4} - 0.1727z^{-5} + 0.02859z^{-6} + 0.003801z^{-7}}{1 - 6.327z^{-1} + 17.63z^{-2} - 28.06z^{-3} + 27.56z^{-4} - 16.7z^{-5} + 5.781z^{-6} - 0.8801z^{-7}}$$

## A.2 Feedforward

System Matrices:

$$A = \begin{bmatrix} 0.9752 & 0.3421 & -0.07598 & -0.6669 & 0.8977 \\ -0.01128 & 0.9184 & -0.8166 & -0.5002 & 1.722 \\ 0.000338 & 0.1704 & 0.8682 & 1.292 & -1.428 \\ 0.001693 & -0.004514 & -0.1086 & 0.8146 & -2.106 \\ -2.869 \cdot 10^{-5} & -0.000823 & -0.002818 & 0.0492 & 0.9329 \end{bmatrix} \quad B = \begin{bmatrix} 0.04258 \\ -0.0002361 \\ -0.002666 \\ 0.0002576 \\ 0.000179 \end{bmatrix}$$

$$C = \begin{bmatrix} 0.3763 & -0.4799 & -0.4982 & 0.4897 & 0.323 \end{bmatrix} \quad D = 0$$

Transfer Function:

$$G(z) = \frac{0.01765z^{-1} - 0.06342z^{-2} + 0.09233z^{-3} - 0.0642z^{-4} + 0.0181z^{-5}}{1 - 4.509z^{-1} + 8.509z^{-2} - 8.402z^{-3} + 4.338z^{-4} - 0.9351z^{-5}}$$

# B. Singular Value Order Analysis

## B.1 Feedback Model

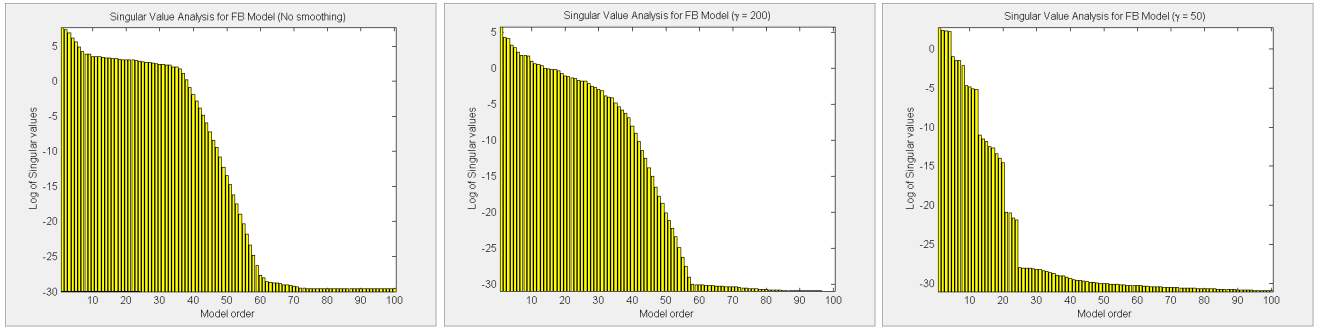


Figure B.1: Singular Value Order Analysis of Different Estimated Smoothed Empirical Transfer Functions (FB Model)

## B.2 Feed-forward Model

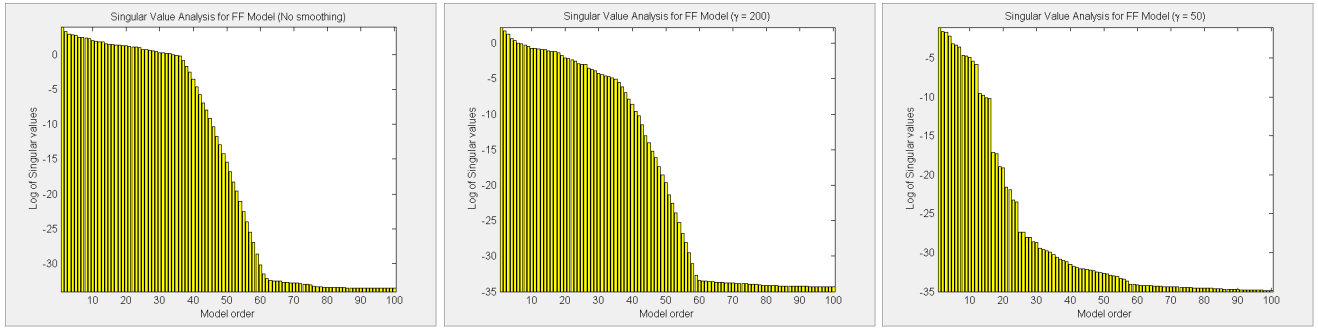


Figure B.2: Singular Value Order Analysis of Different Estimated Smoothed Empirical Transfer Functions (FF Model)

# C. Parameter Optimization

## C.1 Feedback Model

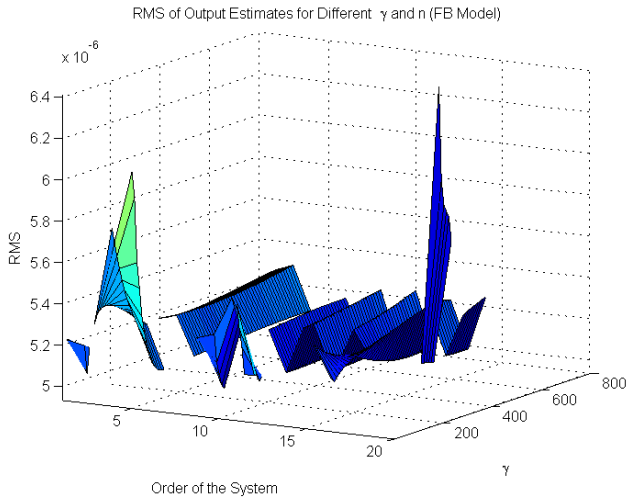


Figure C.1: RMS of the Output Estimate Difference from Stable Feedback System Estimates Derived from Combinations of $\gamma$ and $n$

## C.2 Feed-forward Model

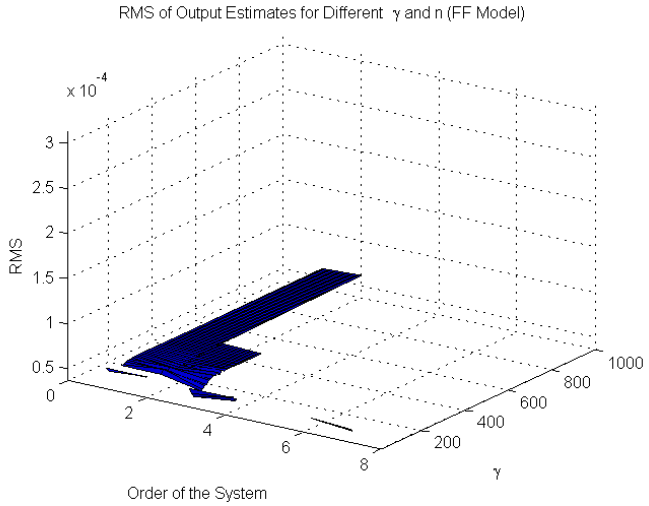


Figure C.2: RMS of the Output Estimate Difference from Stable Feed-forward System Estimates Derived from Combinations of $\gamma$ and $n$

# Bibliography


[1] R Castae-Selga. Active noise hybrid time-varying control for motorcycle helmets. *Control Systems Technology, IEEE Transactions on*, 18(3):602–612, 2010.

[2] Urko Esnaola and Tim Smithers. Mirela: a musical robot. In *Computational Intelligence in Robotics and Automation, 2005. CIRA 2005. Proceedings. 2005 IEEE International Symposium on*, pages 67–72. IEEE, 2005.

[3] D Garcia Violini. Identification and robust active noise control in helmets. *International Journal of Systems Science*, 2014.

[4] Lennart Ljung. *System identification*. Wiley Online Library, 1999.

[5] Tomas McKelvey, Hüseyin Akçay, and Lennart Ljung. Subspace-based multivariable system identification from frequency response data. *Automatic Control, IEEE Transactions on*, 41(7):960–979, 1996.

[6] Peter Van Overschee and Bart De Moor. N4sid: Subspace algorithms for the identification of combined deterministic-stochastic systems. *Automatica*, 30(1):75–93, 1994.

Eidgenössische Technische Hochschule Zürich
Swiss Federal Institute of Technology Zurich
Automatic Control Laboratory

**Title of work:**

# Identification of Acoustic Models for Active Noise Control of Motorcycle Helmets

**Thesis type and date:**

Semester Thesis, March 2014

**Supervision:**

Prof. Dr. Roy S. Smith

**Student:**

Name: Michel D. Heusser
E-mail: mheusser@student.ethz.ch
Legi-Nr.: 07-742-638

**Statement regarding plagiarism:**

By signing this statement, I affirm that I have read and signed the Declaration of Originality, independently produced this paper, and adhered to the general practice of source citation in this subject-area.

Declaration of Originality:

`http://www.ethz.ch/faculty/exams/plagiarism/confirmation_en.pdf`

Zurich, 31. 3. 2014: _____